IEEE Access
Multidisciplinary | Rapid Review | Open Access Journal

Date of publication xxxx 00, 0000, date of current version xxxx 00, 0000.

Digital Object Identifier 10.1109/ACCESS.2017.DOI

Modelling and Simulation of Aerostatic Thrust Bearings

MUHAMMAD PUNHAL SAHTO [1], WANG WEI[1] , LINSHAN HE[1], MUHAMMAD IMRAN[2], LI HAI[1], GONG WEIWEI[1]

[1]School of Mechanical and Electrical Engineering, University of Electronic Science & Technology of China, Chengdu, 611731, China (e-mail: author@boulder.nist.gov)
[2]Mechanical Engineering & Design, School of Engineering and Applied Science, Aston University, B4 7ET, Birmingham, UK (e-mail: author@lamar.colostate.edu)

Corresponding author: First A. Author (e-mail: author@ boulder.nist.gov).

This work is fully funded by National Natural Science Foundation and National Association Security Foundation China (NASF) under Grant No. U183010027.

ABSTRACT This paper demonstrates modeling and simulation comparison of the static characteristics of a porous, orifice, and multiple type aerostatic thrust bearings on the basis of load-carrying capacity(LCC) and stiffness. The Navier-Stokes (N-S) equations are used to solve the internal distribution of pressure in computational fluid dynamics(CFD) simulation environment. An axisymmetric model, which minimizes the computational time and increases efficiency, is used to evaluate the static characteristics of a porous, orifice, and multiple restrictors of aerostatic bearings. Our numerical analysis and empirical results show the agreement with significant affect of material and geometrical parameters on the LCC and stiffness. The thickness of the air film is less than 10μm, the multiple orifice restrictors have more LCC than porous and orifice restrictor. The porous restrictor's stiffness is larger than orifice and multiple restrictors. The LCC of porous and orifice is notably smaller than multiple orifice restrictors. Additionally, it is analyzed that LCC of porous, orifice, and multiple orifice restrictors can be improved with an increase in the supply of air pressure.

INDEX TERMS Enter key words or phrases in alphabetical order, separated by commas.

I. INTRODUCTION

THe aerostatic bearings are used to acquire motion accuracy and minimum friction in numerous measuring machines, lithography equipments, and machine tools. Several kinds of restrictors such as porous, orifice, compound and slot usually used in aerostatic bearings. The porous bearing has an advantage over other restrictors because of its uniform pressure distribution on surface of bearing. Due to this property it has more force, stiffness and stability which are sustained by porous material. Several studies have been initiated for finding characteristics of aerostatic bearings. Uichiro Nishuo et al. [17] has examined the characteristics of aerostatic bearing in experimental and numerical way. The co-efficient of discharge can be numerically found out based on CFD using finite difference method (FDM). The co-efficient of damping and stiffness of restrictors with feed-holes are larger than compound restrictors of bearings. Cui et al. [6] carried out a study on pressure distribution of film, affected the porous aerostatic bearings by manufacturing errors. Jianbo Zhanga et al. [25] analyzed that the depression of pressure is debilitated by increasing diameter of orifice, minimizing the film thickness and pressure supply. Huanga et al. [10] exploit FDM and iterative process to calculate static characteristics with vacuum pre-load thrust aerostatic bearing. Yoshimoto S et al. [23] proposed two air supply methods of annular groove and hole supply to refrain from the deflection. A theoretical study by Yuntang Li and Han Ding [13] showed that the performance of bearing is affected by the pressure of a gas, film thickness, structural design, and diameter of the orifice.

they used FDM and iterative algorithm to minimize iterative times for calculating static characteristics with vacuum pre-load thrust aerostatic bearing

Schenk et al. [19] investigate the effect of gap height and gas load at the vacuum conditions to cause gas flow leakage. Jeng et al. [11] examined stiffness with comparison of single and double pad aerostatic bearings. Hailong Cui et al. [5] revealed that the amplitude errors can rise with the variation

This article has been accepted for publication in a future issue of this journal, but has not been fully edited. Content may change prior to final publication. Citation information: DOI 10.1109/ACCESS.2020.2999748, IEEE Access

of stiffness and load. Wen-Jong Lin et al. [14] also investigate the gas supply, orifice diameter, and bearing surface are the main elements for the performance of air bearing. Cui et al. [4] proposed proportional division method (PDM) and finite element method (FEM) to calculate the angular stiffness. It shows the suitable film thickness corresponds by increasing diameter of orifice. The CFD is adopted to examine the discharge co-efficient without a feed pocket of feed hole. The FDM is used for the analysis of bearing's characteristics [16]. As compared to the other types of aerostatic bearings, the porous aerostatic bearing has better performance in applications of high precision or speed [12] [7] [20]. The static performance of bearing improves with a porous thickness, which is from 6-8mm when the film thickness decreases. A study shows that, as compare to concave errors, the static characteristics of bearing with a convex error of working surface are better [8]. Mathematical methods for source and slip flow are applied to calculate the static characteristics of aerostatic porous bearings [15]. According to D'Arcy law [22] the porous material in which the flow is parallel through a surface of the bearing is taken. As a little drop of gas at the inlet, stiffness improved with multiple restrictors of aerostatic bearings [1]. The literature review indicates that there have been individual studies on porous thrust and orifice restrictor type bearings and provides detail insight into the impacts of different restrictors on LCC, and stiffness of aerostatic bearings. However, to the best of our knowledge, the *comparison between porous thrust and orifice restrictor* type bearing has not yet been reported.

In this paper, we investigate the porous restrictors, orifice, and multiple orifice restrictors. We also compare the stiffness and LCC of aerostatic porous thrust bearings. The LCC and stiffness are determined with an internal distribution of pressure, the fluent CFD is used for internal pressure distribution in the clearance of bearing. The impacts of supply pressure, a diameter of orifice, air film thickness, parameters of the material and on LCC, and stiffness of the porous thrust aerostatic bearings are investigated. We find that an axisymmetric method is effective to minimize time and increase efficiency during the simulation process. The simulation results are validated with experiments. The remaining parts of the paper are arranged in the following sequence, consisting of several tasks as follows:

The numerical modeling sections present the design and mathematical calculation of porous, orifice, and multiple restrictors aerostatic thrust bearings. The performance of bearing is evaluated in the section of modeling for different parameters. The permeability of porous material and load are tested in a section of an experimental setup. The simulated results of porous, orifice, and multiple aerostatic thrust bearings are validated with experimental results in the section of experimental verification with numerical analysis.

II. NUMERICAL MODELLING

This section discusses the preliminaries including restrictors construction, governing equations, and mass flow rate.

A. RESTRICTORS CONSTRUCTION

The basic geometric design of porous restrictors, orifice, and multiple restrictors are depicted in Fig 1. Through a porous material, gas flows to the film of bearing with a supply of pressure, and leaves out from an edge of the film to the atmosphere, as illustrated in Fig 1a. To support the pad, the thrust film was applied, load capacity of bearing was determined by the film thickness. By way of the orifice and multiple restrictors, gas flows to the film and outflows to the atmosphere, as depicted in Fig 1b and 1c, respectively.

B. GOVERNING EQUATIONS

The pressure distribution calculation is into two parts of porous and the film. In the porous material, flow is viscous laminar, and according to Darcy - Forchheimer law, pressure drops as below.

$$\nabla p = -\frac{\mu \bar{u}}{\alpha} \tag{1}$$

Where μ is the kinematic viscosity, α is the permeability co-efficient, ∇p is the change in pressure, and $\bar{u}$ is the vector of velocity.

The change in pressure of x, y, z coordinates of porous section is:

$$\nabla p_x = \sum_{j=1}^{3} \frac{\mu \bar{u}_j \Delta H_x}{\alpha_{xj}}$$

$$\nabla p_y = \sum_{j=1}^{3} \frac{\mu \bar{u}_j \Delta H_y}{\alpha_{yj}}$$

$$\nabla p_z = \sum_{j=1}^{3} \frac{\mu \bar{u}_j \Delta H_z}{\alpha_{zj}} \tag{2}$$

where, α_{xj}, α_{yj}, α_{zj} are the porous material's co-efficient of permeability in the coordinates. The ΔH_x, ΔH_y, ΔH_z are the thicknesses of porous material in the three directions ∇p_x, ∇p_y, ∇p_z are the pressure drop in three directions x, y, z and $\bar{u_j}$ is the velocity in three coordinate directions.

In this paper, the permeability of porous material was taken as isotropic in the manufacturing process, as the cold isostatic pressing was conducted. It means that α_{xj}, α_{yj}, α_{zj} have similar values.

The conservation laws of momentum and mass are given as below:

$$\frac{\partial(\gamma\rho)}{\partial t} + \mathrm{div}(\gamma\rho\vec{u}) = 0 \tag{3}$$

$$\frac{\partial(\gamma\rho u)}{\partial t} + \mathrm{div}(\gamma\rho\vec{u} \times u) = -\gamma\nabla p \tag{4}$$

As γ is the porosity, ρ is the density of the gas, and t is the time.

The motion of fluid is mostly governed by conservation laws of mass, energy, and momentum in fluid mechanics; which can be formed by N-S equations. The continuity equation is also familiar as the conservation law of mass, is given as:

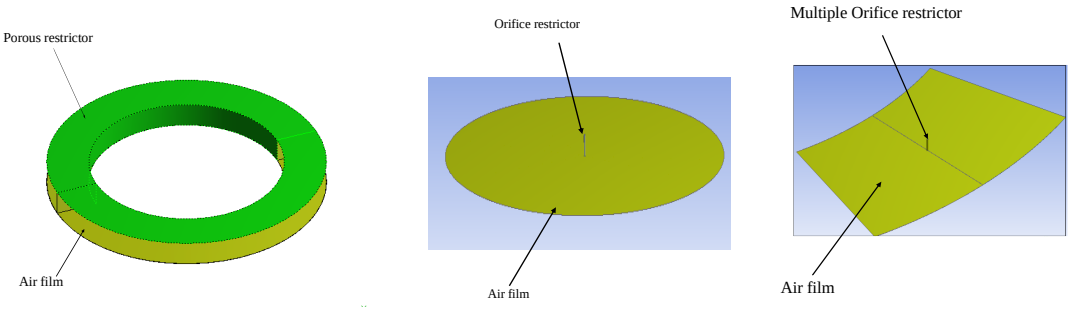

(a) (b) (c)

FIGURE 1: Geometrical construction of different types of restrictors.

$$\frac{\partial \rho}{\partial t} + \frac{\partial(\rho u)}{\partial x} + \frac{\partial(\rho v)}{\partial y} + \frac{\partial(\rho w)}{\partial z} = 0 \tag{5}$$

$$\frac{\partial \rho}{\partial t} + \mathrm{div}(\rho \vec{u}) = 0 \tag{6}$$

where, ρ is the gas density, t is time, and $\bar{u}$ is the vector velocity of cartesian coordinates $(x, y,$ and $z)$, components of velocity $u, v,$ and w are in the 3 coordinate directions. As Newton's second law states, that the equation for conservation of momentum in directions of x, y, z is derived as:

$$\begin{cases} \frac{\partial(\rho u)}{\partial t} + div(\rho \vec{u} u) = -\frac{\partial p}{\partial x} + \frac{\partial \tau_{xx}}{\partial x} + \frac{\partial \tau_{yx}}{\partial y} + \frac{\partial \tau_{zx}}{\partial z} + F_x, \\ \frac{\partial(\rho v)}{\partial t} + \mathrm{div}(\rho \vec{u} v) = -\frac{\partial p}{\partial y} + \frac{\partial \tau_{xy}}{\partial x} + \frac{\partial \tau_{yy}}{\partial y} + \frac{\partial \tau_{zy}}{\partial z} + F_y, \\ \frac{\partial(\rho w)}{\partial t} + div(\rho u w) = -\frac{\partial p}{\partial z} + \frac{\partial \tau_{xz}}{\partial x} + \frac{\partial \tau_{yz}}{\partial y} + \frac{\partial \tau_{zz}}{\partial z} + F_z \end{cases} \tag{7}$$

Here, ρ is pressure of film, τ is the fluid viscous stress, F_x is the force towards x-direction, F_y is force on body towards y-direction, and F_z is force on body towards z direction.

The τ is proportional to the fluid deformation, derived as [3]:

$$\begin{cases} \tau_{xx} = 2\mu \frac{\partial u}{\partial x} + \lambda div(\vec{u}); \tau_{xy} = \tau_{yx} = \mu \left(\frac{\partial u}{\partial y} + \frac{\partial v}{\partial x} \right) \\ \tau_{yy} = 2\mu \frac{\partial v}{\partial x} + \lambda div(\vec{u}); \tau_{xz} = \tau_{zx} = \mu \left(\frac{\partial u}{\partial z} + \frac{\partial w}{\partial x} \right) \\ \tau_{zz} = 2\mu \frac{\partial w}{\partial x} + \lambda div(\vec{u}); \tau_{yz} = \tau_{zy} = \mu \left(\frac{\partial u}{\partial z} + \frac{\partial w}{\partial y} \right) \end{cases} \tag{8}$$

Where dynamic viscosity is μ, and $\lambda = -\frac{2}{3}$.

According to the thermodynamics 1st law, the law of energy conservation is given by :

$$\frac{\partial(\rho T)}{\partial t} + \mathrm{div}(\rho \vec{u} T) = \mathrm{div}\left(\frac{k}{c_p} \mathrm{grad}\, T \right) + \mathrm{S} \tag{9}$$

Where k is the co-efficient of heat transfer of fluid, $gradT$ is the gradient of temperature, specific heat capacity is c_p , and viscous dissipation energy is S.

By solving equations 6, 7, 8, and 9, the distribution of pressure in the clearance of bearing of orifice restrictors can be gained. The distribution of pressure of porous thrust aerostatic bearings can be attained by solving equations, 1,2,3,4, and 9.

C. THE RATE OF MASS FLOW THROUGH AN ORIFICE

The configuration of the thrust aerostatic bearing, in which the orifices are used as restrictors. One row of orifices is evenly and equally spaced put around the bearing circumference. Taking into account, the flow through an orifice, bellow suppositions have been obtained [18]:

- The losses are not of upstream pressure of the jet throat, i.e. the p_s is supply pressure of jet at entry.
- The static pressure of the jet in the throat quickly goes down.

In general, the rate of mass flow of gas through the orifice is produced as an ideal nozzle. Since the pressure supply p_s is decreased p_d through an orifice. Derived from the ideal mass flow rate [21]:

$$m_r = C_d \times m_t \tag{10}$$

$$m_r = A P_S \sqrt{\frac{2\rho a}{P_a} \Psi_r} \quad \because A = \frac{\pi d^2}{4} \tag{11}$$

Where P_a is the atmospheric pressure. d is the diameter of orifice, P_d is the outlet pressure of orifice, P_s is the pressure supply, specific heat ratio is the k, and $k = 1.4$ is the value for gas, ρ is the gas density, in actual condition m_r is the rate of mass flow, m_t is the theoretical rate of mass flow, and C_d is the co-efficient of discharge. And Ψ_s is the function of mass flow and is described as bellow

This article has been accepted for publication in a future issue of this journal, but has not been fully edited. Content may change prior to final publication. Citation information: DOI 10.1109/ACCESS.2020.2999748, IEEE Access

$$\Psi_s = \begin{cases} \left[K/2(2/K+1)^{(K+1)/(K-1)}\right]^{1/2}; \\ \mathrm{P_d}/P_s \le (2/K+1)^{K/(K+1)} \\ \\ \left\{K/K-1\left[(P_d/P_s)^{2/k} - (P_d/P_s)^{(k+1)/k}\right]\right\}^{1/2}, \\ P_d/P_s > (2/K+1)^{K/(K+1)} \end{cases} \tag{12}$$

By solving equations 10-12 flow of gas mass through an orifice can be obtained. Fig 2 shows a flow chart, calculation of static characteristics of a thrust bearing.

III. METHOD OF CALCULATION

Characteristics of flow field calculated of aerostatic bearings by using key methods that are FEM and FDM [9]. However, FEM and FDM cannot effectively solve the N-S equations. In this article, based on the CFD, FLUENT 16.0 is used to resolve N-S equations. The fluent is selected to calculate the equations for viscous laminar. In this research, mass flow rate is very small through porous. Hence, the model is a laminar described in the viscous state. An axisymmetric model is used to minimize the time during a simulation.

A. GRIDS CALCULATION

In numerous antecedent research, the aerostatic pad bearings design was made simple to the symmetric model [2]. The boundary conditions and grids utilized for porous and orifice restrictors are shown in Fig 3. In this paper, for minimizing the time and to increase the computation efficacy, the axisymmetric model is applied to evaluate characteristics of porous, orifice, and multiple restrictors aerostatic circular pad bearings, as depicted in Fig 3a, 3b, and 3c, respectively. The model is selected as periodic axisymmetric for the orifice restrictors as depicted in Fig 3, and for the calculations slice of the geometric structure is essential. Before calculation, to confirm the validity of simulation results, the independence of gird must be verified. For the computation of the different types of restrictors, the conditions used as stated in Table 1.

IV. EXPERIMENTAL SETUP

A. TEST OF PERMEABILITY OF POROUS MATERIAL

The permeability co-efficients are majorly efrecting on the CFD results and performance of porous bearings. The permeability co-efficient gives consideration throttle performance of the restrictor, which changes from $10^{-6}\mathrm{m}^2$ to $10^{-15}\mathrm{m}^2$. In Fig 4. the porous material is utilized by test equipment to acquire the permeability co-efficient with a diameter of $80\mathrm{mm}$ and thickness of $8\mathrm{mm}$, porous graphite material is the measured specimen. The test platform comprises on precision pressure regulating valve, gas tank, flowmeter, fixture, porous material, voltage line, pneumatic pipeline, and dried, pressurizes air supply system, etc.

The gas flow and its flow-rate are measured by the flowmeter. The pressure sensor is used for measuring pressure. The

TABLE 1: Computational conditions and input parameters of CFD for different restrictors

Computational conditions and design variable	Value
Viscosity Flow	Laminar
Inertia co-efficient	2.58e+5 1/m
Fluid	Ideal gas
Temperature	293 K
Method of solution	Simple C
Solution standardization	Standard initialization
Atmospheric pressure	101.325 k Pa
Supply pressure	0.4 MPa/ 0.5 MPa/ 0.6 MPa
Specific heat	1.00643 kJ/(kg.K)
Outlet pressure	0 MPa
Inside diameter	56000 μm
Outside diameter	80000 μm
Rows of orifices	1
Location of orifice row	68000 μm
Number of orifices	12
Diameter of orifice	0.05-0.15mm
Co-efficient of viscous resistance	1.27e+14 m-2
Dynamic Viscosity	$1.789e^{-5}s$kg/(m-s)
Porosity	0.18
Bearing thickness H	6mm/8mm/10mm
Thickness of gas film	20 μm

pressure change and flow-rate give the internal flow of the material, as shown in Fig 5.

In Fig 5 relation between change in pressure and rate of flow is linear and fulfills the condition of Darcy-Forchheimer law. The gas flows through porous material governed by law of Darcy-Forchheimer, given as below.

$$\Psi = \frac{Q\eta H}{\Delta pa} \tag{13}$$

Where a is the surface area along the direction of gas flow, η is the kinematic viscosity of gas, Δp_{is} the change in pressure between front and back porous material surface, H is the thickness of porous material and Ψ is the co-efficient of permeability of porous material. Q is volume flow through porous material.

B. LOAD CAPACITY TESTS OF POROUS THRUST AEROSTATIC BEARINGS

The LCC of porous thrust aerostatic bearings is measured by the experimental setup. To reduce the environmental disruption, the equipment of measurement is put on a platform of vibration isolation. The static performance test platform comprises of load precision pressure regulating valve, porous thrust bearings, fixture, gas tank, flow meter, pneumatic pipeline, etc. The load applied to porous thrust aerostatic

This article has been accepted for publication in a future issue of this journal, but has not been fully edited. Content may change prior to final publication. Citation information: DOI 10.1109/ACCESS.2020.2999748, IEEE Access

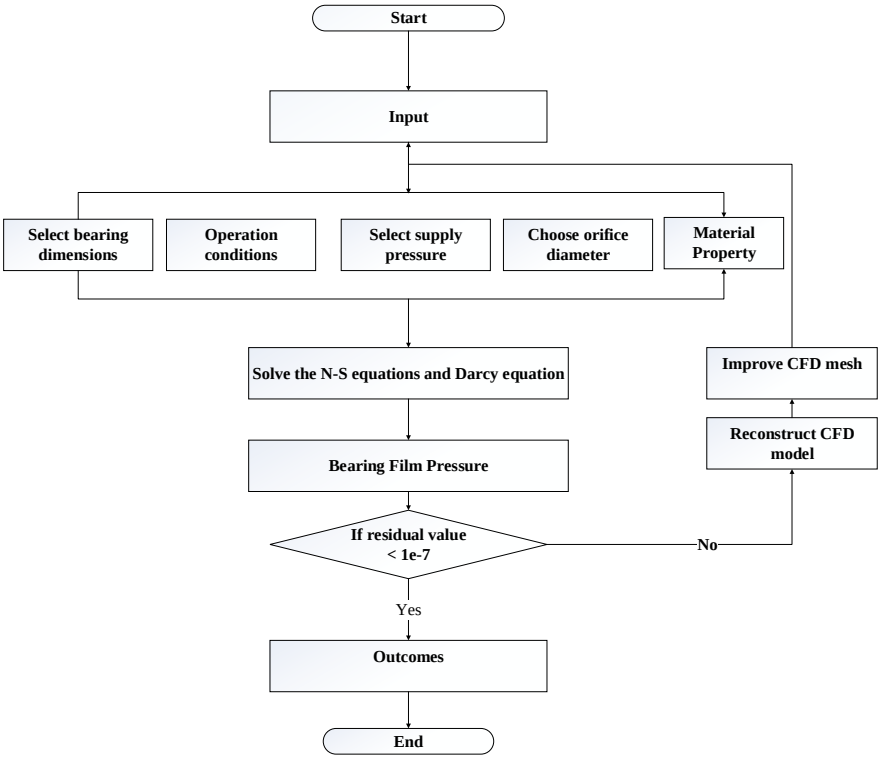

FIGURE 2: The flow chart determining the load capacity and stiffness.

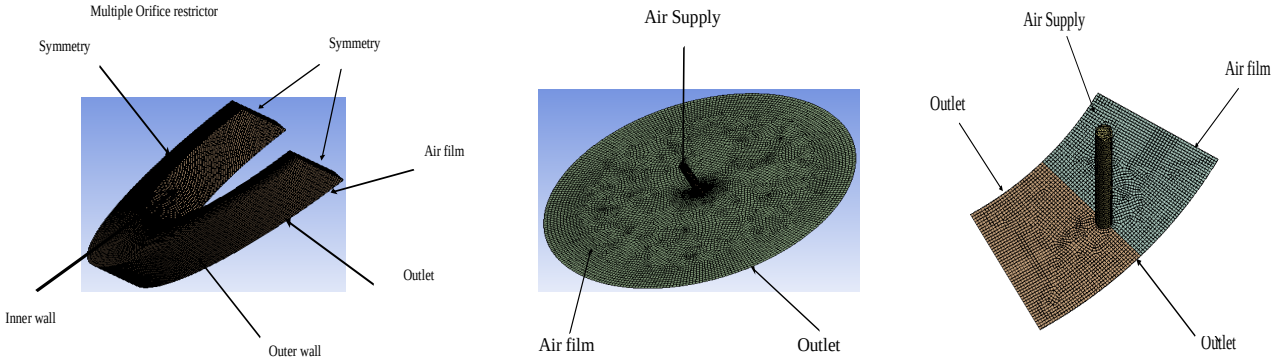

(a) porous (b) orifice (c) multiple orifice

FIGURE 3: Mesh model of aerostatic thrust bearing.

bearings is measured by load transducers. The displacement sensors are used to measure a change in the thickness of a film.

V. EXPERIMENTAL VERIFICATIONS WITH NUMERICAL ANALYSIS

A. EXPERIMENTAL VALIDATION

The experimental LCC results of porous aerostatic bearing are depicted in Fig 6. The results of experiment indicate the agreement with simulated results, therefore validating numerical method applied in this paper.

The 17.11% of LCC of porous aerostatic thrust bearing is the maximum variance between the results of experiments and simulation. The benefit of porous restrictor is better when the film thickness is below 5μm. LCC is decreasing with an increase of film thickness, and with the supply of 0.4 MPa pressure. With a 0.5 MPa supply of pressure, the load capacity is more than 0.4MPa

B. NUMERICALLY ANALYSIS

In this study, the viscous laminar, ideal gas model, CFD, and SIMPLEC are chosen in the FLUENT software. In

This article has been accepted for publication in a future issue of this journal, but has not been fully edited. Content may change prior to final publication. Citation information: DOI 10.1109/ACCESS.2020.2999748, IEEE Access

Table 1, the boundary conditions and geometrical parameters are given. The LCC of porous aerostatic bearings decreases with increase of air film thickness, whereas, with increasing thickness of porous, LCC decreases, while the LCC increases with the increase of supply pressure. The LCC is smaller with a smaller co-efficient of permeability. The LCC gradually decreases when the 15μm is thickness of film, while the porous thickness is 6 mm when the thickness of an air film is 5μm, the load is high. For keeping a comparatively high load of bearings under the minimum usage of gas, it requires to reduce a diameter of porous restrictor aerostatic bearing. The load-carrying capacity is delicate to vary in diameter.

In Fig 8, aerostatic bearing stiffness decreases, when the thickness of air film decreases. The porous restrictor thickness can affect the stiffness of aerostatic bearings. The stiffness increases, as the porous restrictor thickness increases. The bearings have different stiffness relative to varying air film thickness. The stiffness is delicate to vary in thickness. The high value of stiffness can be obtained with a large thickness of porous thickness. To determine the porous aerostatic bearings performance, the material permeability is the key parameter. Generally, it is taken between $10^{-14}m^2$ and $10^{-12}m^2$ [24].

The rate of mass flow increasing with decreasing of porous thickness as shown in Fig 9. The flow of mass is especially affected by the variation of porous thickness, diameter, and film thickness of porous restrictor, whereas the thickness of film is more affecting on stiffness. Generally, it is easy to guarantee the accuracy of impact machinery with air film thickness greater than 15μm, but if its restrictor thickness is too low, the restrictor may be damaged. [26]. The boundary conditions for orifice type aerostatic bearings are same as for porous aerostatic bearings. The static characteristics of orifice type bearings were gotten by using CFD Fluent. In Fig 10, the LCC increases as the thickness of air film decrease, but the bearings have different load-carrying capacity with different diameters of orifice. With an increasing diameter of orifice increases, LCC increases. The LCC decreases as thickness of air film is more than 15μm but increases with increasing of air pressure.

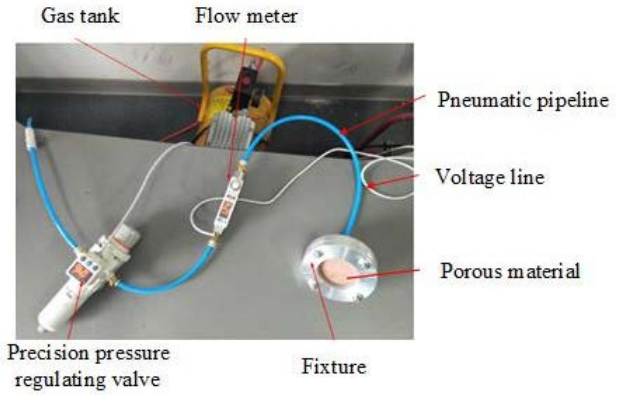

FIGURE 4: Experimental setups for the permeability of porous material.

The thickness of air film increases, stiffness first increases, and then decreases as shown in Fig 11. While the orifice diameter increases, but the stiffiness decreases. At different sizes of a diameter of orifices have varying values of stiffness relative to different values of air film thickness. The stiffness is lesser when the diameter of an orifice is 0.5mm. Though, when the thickness of air film is between 5μm and 15μm, the stiffiness is high, and then decreases uniformly. Though, while the diameter of the orifice is less than 100μm, an optimum thickness of air film is less than 10μm, which creates processing very hard. In this section, it can be concluded that bearings can take full advantage when working between 10μm and 15μm.

Fig 12 depicts the mass flow increases, as the air film decreases. When the orifice diameter increases, the mass flow of gas decreases. The multiple restrictors are usually designed to upkeep the load of the aerostatic bearing. So, the number of restrictors certainly is the key factor for the bearing objective. The 80mm and 56mm are the outside diameters and inside diameter of the aerostatic thrust bearing respectively. The orifices are placed around a circle of reference diameter of 68mm. The boundary conditions were used the same for multiple restrictors.

The characteristics of aerostatic thrust bearing with multiple orifices as illustrated in Fig 13. The LCC of the bearing can increase with an increasing number of orifices. The LCC of multiple restrictors increases when the orifice diameter increases.

As depicted in Fig 14. the maximum stiffness of aerostatic thrust bearing decreases as an increasing number of orifices. While stiffness increases, when the diameter of orifice decreases. The thickness of air film increases, stiffness first increases and then decreases. The maximum stiffness of multiple orifices is between 10μm and 15μm. When the supply of air pressure is increasing, the stiffness also increases.

As the mass flow increases, while the number of orifice increases, as shown in Fig 15. Due to maximum pressure supply, the flow of mass is maximum, but a minimum consumption of gas is, as the air film thickness decreases. As the diameter of orifice decreases, mass flow decreases, but for a large diameter of orifice, the gas consumption is high.

The comparison of three types of restrictors reveals that as 5μm is film thickness, LCC of the porous is 8.8% greater than single orifice, but the stiffiness is nearly the same when the thickness of air film is 15 μm. The LCC of multiple orifice restrictors is larger than both porous and single orifice restrictor aerostatic bearings. An increasing number of orifices, the stiffiness can increase than the porous bearings. The multiple orifice restrictor's stiffnesses are larger than the porous restrictor when the film thickness is 10μm

VI. CONCLUSION AND FUTURE WORK

This work investigates the advantages and disadvantages, which are based on the factors optimization of porous and

This article has been accepted for publication in a future issue of this journal, but has not been fully edited. Content may change prior to final publication. Citation information: DOI 10.1109/ACCESS.2020.2999748, IEEE Access

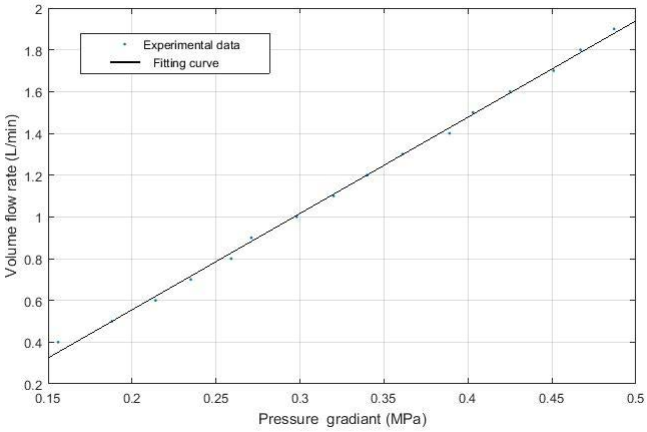

FIGURE 5: The relation of pressure and rate of flow of porous material

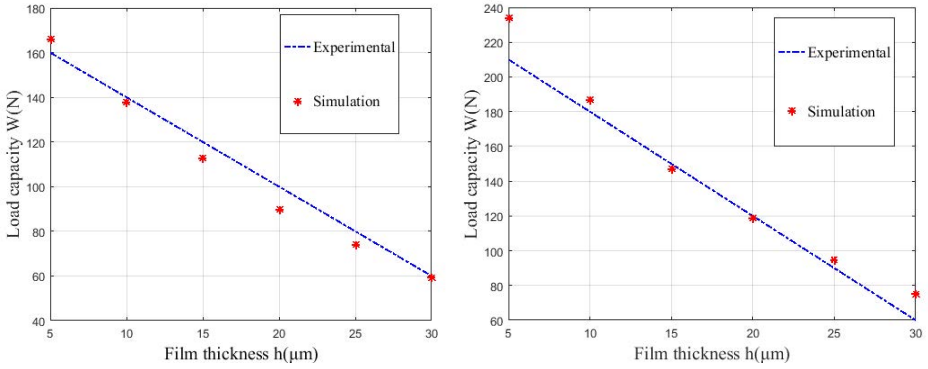

(a) Load capacity 0.4MPa (b) Load capacity 0.5MPa

FIGURE 6: Experimental and simulation results of porous aerostatic thrust bearings.

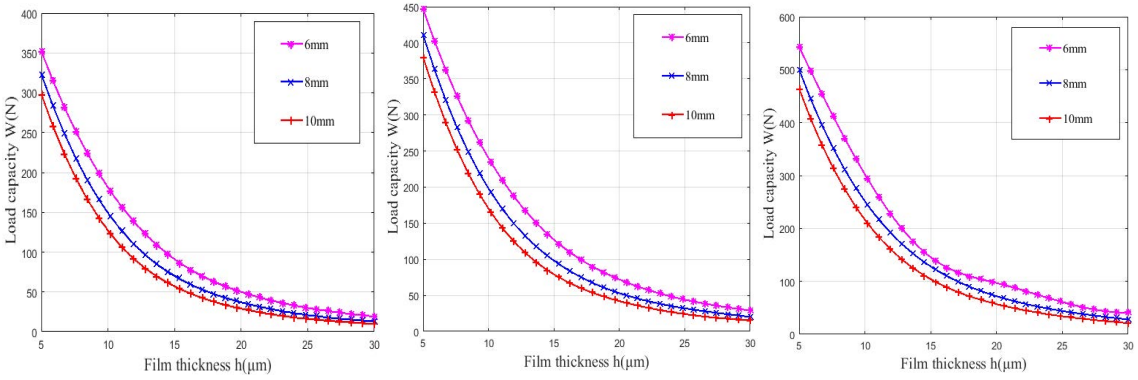

(a) Load capacity 0.4MPa (b) Load capacity 0.5MPa (c) Load capacity 0.5MPa

FIGURE 7: Load capacity versus film thickness (h) of porous restrictor of the bearings.

orifice type bearings. Several findings are given as follows. The stiffness of porous restrictors regularly decreases by reducing the thickness of porous; for single and multiple orifice restrictors, it slowly rises at the highest value then declines with an increase of thickness of air film. The material and geometrical factors are effecting meaningfully on aerostatic bearing's stiffness.

The multiple restrictors have stiffness ominously better than single orifice restrictor. When the thickness of air film is less than 5μm, the porous restrictors have benefits for stiff-

This article has been accepted for publication in a future issue of this journal, but has not been fully edited. Content may change prior to final publication. Citation information: DOI 10.1109/ACCESS.2020.2999748, IEEE Access

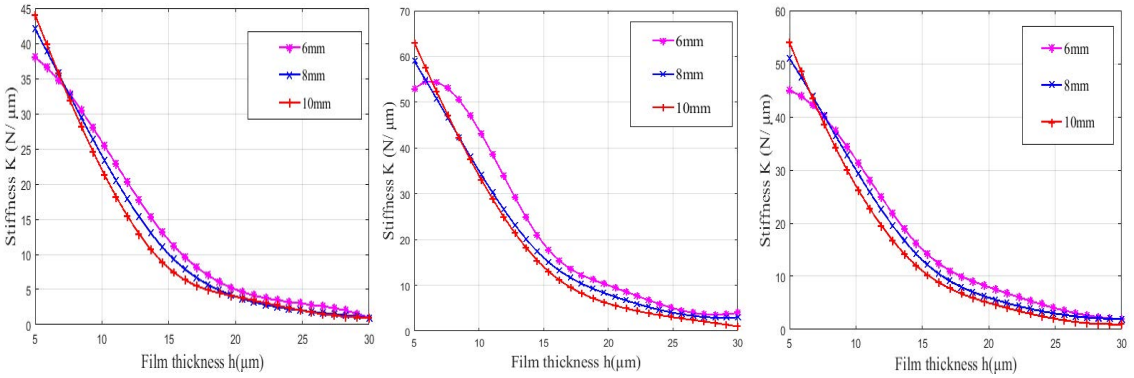

(a) (b) (c)

FIGURE 8: Stiffness versus film thickness (h) of porous restrictor of the bearing.

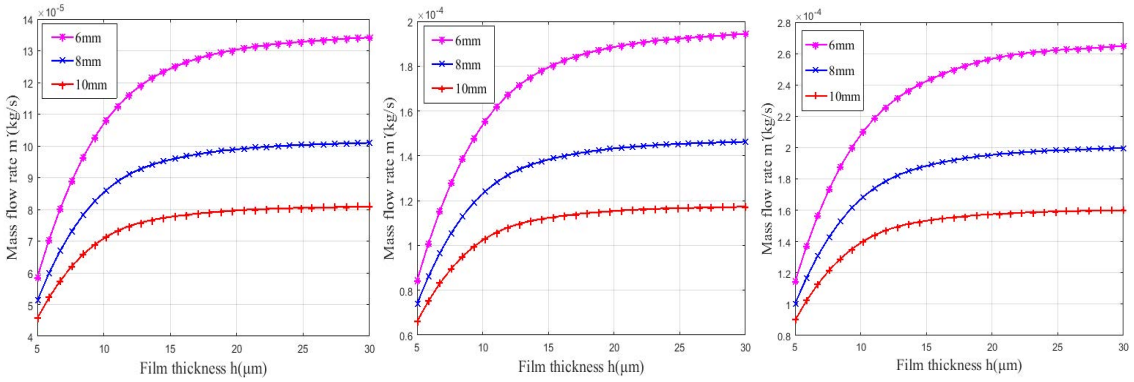

(a) (b) (c)

FIGURE 9: Mass flow versus film thickness (h) of porous restrictor of the bearings.

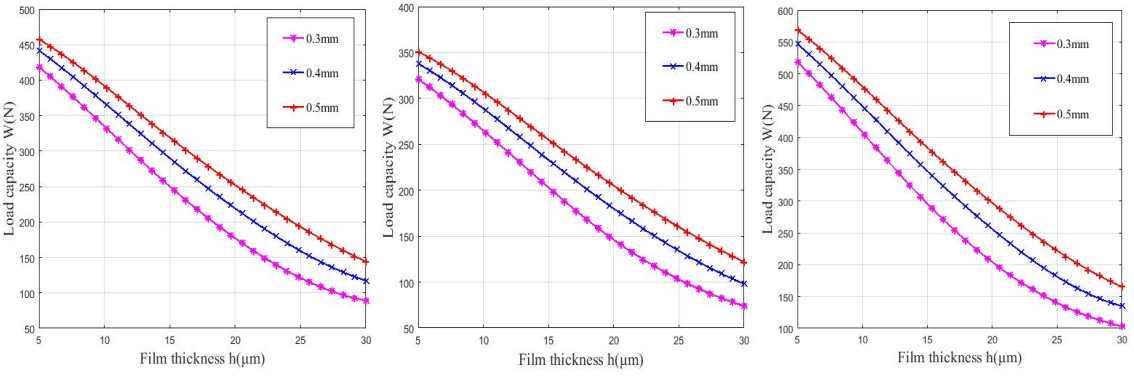

(a) (b) (c)

FIGURE 10: Load capacity versus film thickness (h) of orifice restrictor of the bearings.

This article has been accepted for publication in a future issue of this journal, but has not been fully edited. Content may change prior to final publication. Citation information: DOI 10.1109/ACCESS.2020.2999748, IEEE Access

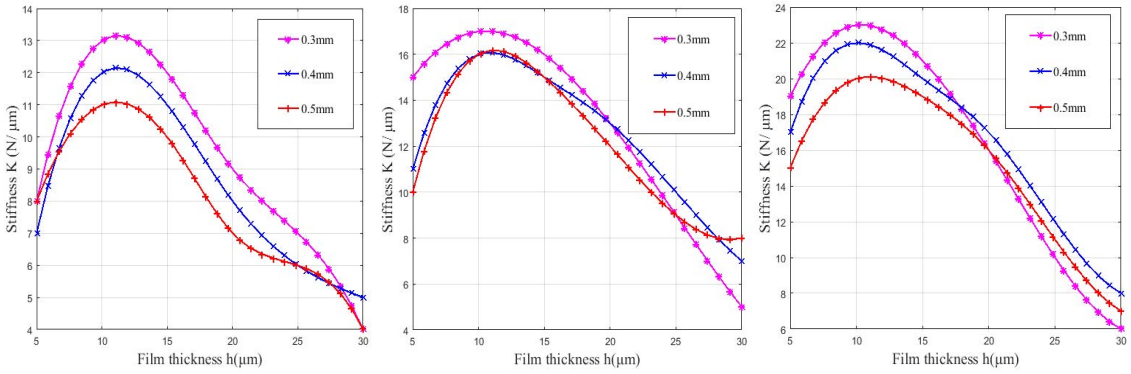

(a) (b) (c)

FIGURE 11: Stiffness versus film thickness (h) of orifice restrictor of the bearings.

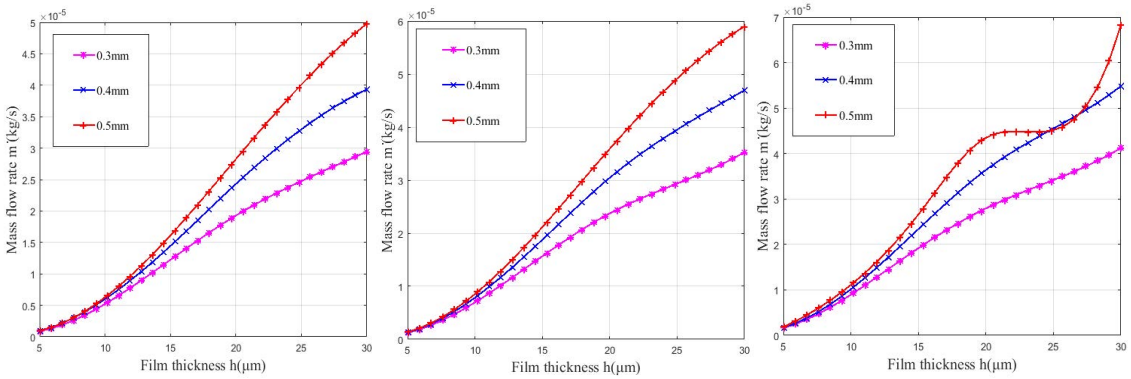

(a) (b) (c)

FIGURE 12: Mass flow versus film thickness (h) of orifice restrictor of the bearings.

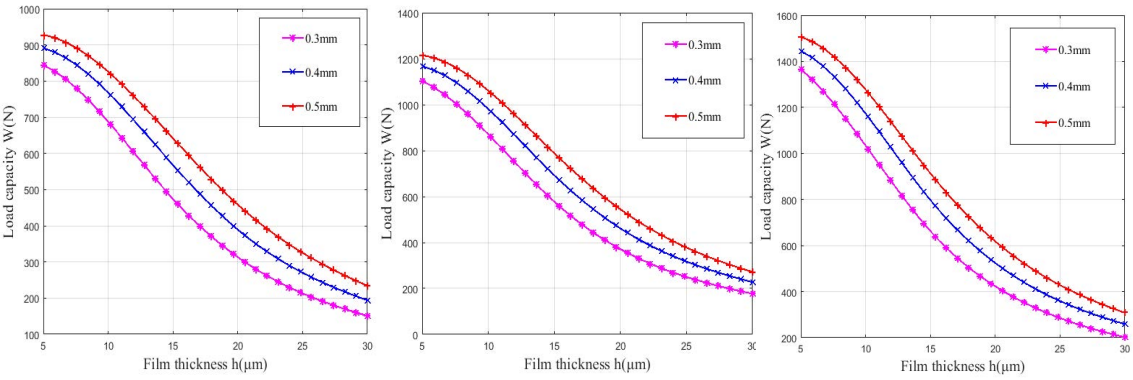

(a) (b) (c)

FIGURE 13: Load capacity versus film thickness (h) of multiple orifice restrictor of the bearings.

ness. Therefore, the stiffness of porous is better as compared to a single orifice restrictor. The LCC of multiple orifice restrictors is larger than porous and single orifice restrictors. The multiple orifice restrictors have more load capacity than porous and single orifice restrictor if the air film thickness is less than 10μm, The stiffness and LCC of porous, single and multiple orifice restrictors can be improved by increasing gas pressure. The stiffness of aerostatic thrust bearings is better as a diameter of multiple orifice restrictors decreases. This work is based on the experimental and simulation design of porous aerostatic thrust bearing. Simulation is performed for orifice and multiple orifice aerostatic thrust bearing. In the

This article has been accepted for publication in a future issue of this journal, but has not been fully edited. Content may change prior to final publication. Citation information: DOI 10.1109/ACCESS.2020.2999748, IEEE Access

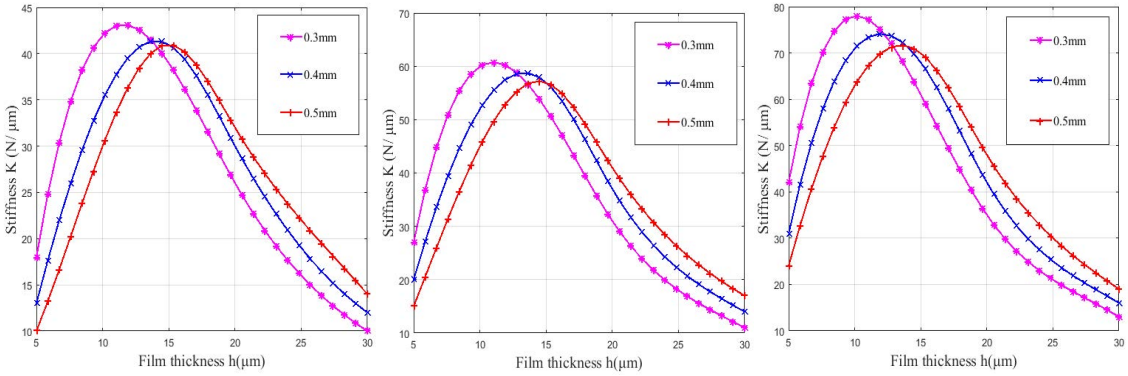

(a) (b) Stiffness 0.5MPa (c)

FIGURE 14: Stiffness versus film thickness (h) of multiple orifice restrictor of the bearings.

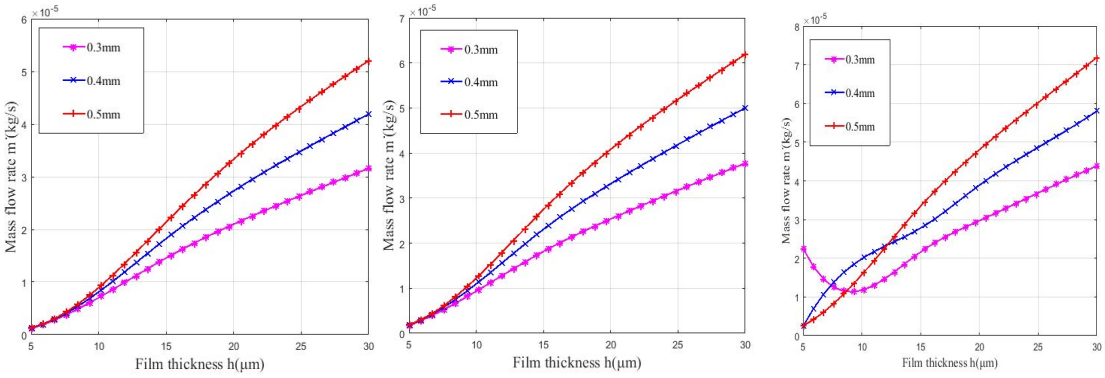

(a) (b) (c)

FIGURE 15: Mass flow versus film thickness(h) of multiple orifice restrictor of the bearings.

future we aim to conduct an experimental study on the orifice and multiple orifice restrictor bearings.

.

Appendixes, if needed, appear before the acknowledgment.

ACKNOWLEDGMENT

This work is fully funded by National Natural Science Foundation and National Association Security Foundation China (NASF) under Grant No. U183010027.

APPENDIX A REFERENCE EXAMPLES

REFERENCES

[1] A. Charki, K. Diop, S. Champmartin, and A. Ambari, "Numerical simulation and experimental study of thrust air bearings with multiple orifices," International Journal of Mechanical Sciences, vol. 72, pp. 28–38, 2013.

[2] X.-D. Chen and X.-M. He, "The effect of the recess shape on performance analysis of the gas-lubricated bearing in optical lithography," Tribology international, vol. 39, no. 11, pp. 1336–1341, 2006.

[3] H.-L. Cui, Y. Wang, B.-R. Wang, H. Yang, and H. Xia, "Numerical simulation and experimental verification of the stiffness and stability of thrust pad aerostatic bearings," Chinese Journal of Mechanical Engineering, vol. 31, no. 1, pp. 1–12, 2018.

[4] H. Cui, Y. Wang, H. Yang, L. Zhou, H. Li, W. Wang, and C. Zhao, "Numerical analysis and experimental research on the angular stiffness of aerostatic bearings," Tribology International, vol. 120, pp. 166–178, 2018.

[5] H. Cui, Y. Wang, X. Yue, M. Huang, and W. Wang, "Effects of manufacturing errors on the static characteristics of aerostatic journal bearings with porous restrictor," Tribology International, vol. 115, pp. 246–260, 2017.

[6] H. Cui, Y. Wang, X. Yue, M. Huang, W. Wang, and Z. Jiang, "Numerical analysis and experimental investigation into the effects of manufacturing errors on the running accuracy of the aerostatic porous spindle," Tribology International, vol. 118, pp. 20–36, 2018.

[7] M. Fourka and M. Bonis, "Comparison between externally pressurized gas thrust bearings with different orifice and porous feeding systems," Wear, vol. 210, no. 1-2, pp. 311–317, 1997.

[8] Y. Hechun, L. Huanhuan, Z. Huiying, and M. Wenqi, "Research on the static characteristics of circular thrust porous aerostatic bearings," in 2015 IEEE International Conference on Mechatronics and Automation (ICMA). IEEE, 2015, pp. 1407–1411.

[9] J. Huang, J. Zhang, W. Shi, and Y. Wang, "3d fem analyses on flow field characteristics of the valveless piezoelectric pump," Chinese Journal of Mechanical Engineering, vol. 29, no. 4, pp. 825–831, 2016.

[10] M. Huang, Q. Xu, M. Li, B. Wang, and J. Wang, "A calculation method on the performance analysis of the thrust aerostatic bearing with vacuum pre-load," Tribology International, vol. 110, pp. 125–130, 2017.

[11] Y.-R. Jeng and S. Chang, "Comparison between the effects of single-pad and double-pad aerostatic bearings with pocketed orifices on bearing stiffness," Tribology International, vol. 66, pp. 12–18, 2013.

[12] Y. P. KWAN and J. Corbett, "Porous aerostatic bearings: an updated review," Wear, vol. 222, no. 2, pp. 69–73, 1998.

[13] Y. Li and H. Ding, "A simplified calculation method on the performance

analysis of aerostatic thrust bearing with multiple pocketed orifice-type restrictors," Tribology international, vol. 56, pp. 66–71, 2012.

[14] W.-J. Lin, J. P. Khatait, W. Lin, and H. Li, "Modelling of an orifice-type aerostatic thrust bearing," in 2006 9th International Conference on Control, Automation, Robotics and Vision. IEEE, 2006, pp. 1–6.

[15] T. Luong, W. Potze, J. Post, R. Van Ostayen, and A. Van Beek, "Numerical and experimental analysis of aerostatic thrust bearings with porous restrictors," Tribology International, vol. 37, no. 10, pp. 825–832, 2004.

[16] M. Miyatake and S. Yoshimoto, "Numerical investigation of static and dynamic characteristics of aerostatic thrust bearings with small feed holes," Tribology International, vol. 43, no. 8, pp. 1353–1359, 2010.

[17] U. Nishio, K. Somaya, and S. Yoshimoto, "Numerical calculation and experimental verification of static and dynamic characteristics of aerostatic thrust bearings with small feedholes," Tribology International, vol. 44, no. 12, pp. 1790–1795, 2011.

[18] J. W. Powell, "Design of aerostatic bearings," 1970.

[19] C. Schenk, S. Buschmann, S. Risse, R. Eberhardt, and A. Tünnermann, "Comparison between flat aerostatic gas-bearing pads with orifice and porous feedings at high-vacuum conditions," Precision Engineering, vol. 32, no. 4, pp. 319–328, 2008.

[20] ——, "Comparison between flat aerostatic gas-bearing pads with orifice and porous feedings at high-vacuum conditions," Precision Engineering, vol. 32, no. 4, pp. 319–328, 2008.

[21] L. Song, K. Cheng, H. Ding, and S. Chen, "Analysis on discharge coefficients in fem modeling of hybrid air journal bearings and experimental validation," Tribology International, vol. 119, pp. 549–558, 2018.

[22] Y. Tian, "Static study of the porous bearings by the simplified finite element analysis," Wear, vol. 218, no. 2, pp. 203–209, 1998.

[23] S. Yoshimoto and K. Kohno, "Static and dynamic characteristics of aerostatic circular porous thrust bearings (effect of the shape of the air supply area)," J. Trib., vol. 123, no. 3, pp. 501–508, 2001.

[24] L. Zesheng, D. Jinming, and S. Yazhou, "Analysis on aerostatic porous spherical bearings static performance," Chinese Journal of Mechanical Engineering, vol. 40, pp. 115–119, 2004.

[25] J. Zhang, D. Zou, N. Ta, and Z. Rao, "Numerical research of pressure depression in aerostatic thrust bearing with inherent orifice," Tribology International, vol. 123, pp. 385–396, 2018.

[26] X. F. Zhang and B. Lin, "Theoretical research on deformation of porous material in air bearing," in Applied Mechanics and Materials, vol. 215. Trans Tech Publ, 2012, pp. 779–784.

FIRST A. AUTHOR (M'76–SM'81–F'87)